

## Dielectric and magnetic anomalies and spin frustration in hexagonal $RMnO_3$ ( $R=Y, Yb,$ and $Lu$ )

T. Katsufuji,<sup>1,2</sup> S. Mori,<sup>3</sup> M. Masaki,<sup>1</sup> Y. Moritomo,<sup>4</sup> N. Yamamoto,<sup>3</sup> and H. Takagi<sup>1,2</sup>

<sup>1</sup>*Department of Advanced Materials Science and Department of Applied Chemistry, University of Tokyo, Tokyo 113-8656, Japan*

<sup>2</sup>*Core Research for Evolutional Science and Technology (CREST), Japan Science and Technology Corporation, Japan*

<sup>3</sup>*Department of Physics, Tokyo Institute of Technology, Tokyo 152-8551, Japan*

<sup>4</sup>*CIRSE and Department of Crystalline Materials Science, Nagoya University, Nagoya 464-8601, Japan*

(Received 25 May 2001; published 22 August 2001)

Single crystals of hexagonal  $RMnO_3$  ( $R=Y, Yb,$  and  $Lu$ ), where Mn ions form the triangular lattice, were investigated, focusing on their dielectric/magnetic anomalies as well as geometrical spin frustration. It is found that the ratio of a Weiss temperature to  $T_N$  is  $\sim 10$  in  $RMnO_3$ , indicating the dominant role of strong geometrical frustration. The effect of geometrical frustration also appears in specific heat, which shows a presence of a substantial amount of residual magnetic contribution below  $T_N$ , indicating that a part of the spins are still fluctuating at  $T \ll T_N$ . It is also found that the dielectric anomaly at  $T_N$  is strongly anisotropic, suggesting a unique correlation between magnetism and dielectric properties in these compounds.

DOI: 10.1103/PhysRevB.64.104419

PACS number(s): 75.80.+q, 75.40.-s, 77.80.-e, 61.14.-x

### I. INTRODUCTION

$RMnO_3$  ( $R$  is rare earth) crystallizes in a hexagonal structure when the ionic radius of  $R$  is small ( $R=Ho-Lu, Y,$  and  $Sc$ ). In this hexagonal structure, each  $Mn^{3+}$  ion with  $S=2$  is surrounded by three in-plane and two apical oxygen ions, and thus is subject to a trigonal crystal field. These  $MnO_5$  blocks are two-dimensionally connected with each other on their corners, and the triangular lattice of the  $Mn^{3+}$  ions is formed, as shown in Fig. 1. Based on such a triangular lattice, these compounds experience several characteristic distortions. One is Mn “trimers” (i.e.,  $\sqrt{3} \times \sqrt{3}$  ordering), which are characterized by the shift of three  $Mn^{3+}$  ions surrounding one oxygen ion toward the oxygen, as shown on the right side of Fig. 1.<sup>1</sup> Another one is the displacement of ions along the  $c$  axis (perpendicular to the triangular-lattice plane) causing a ferroelectric polarization.<sup>2</sup> Since the ferroelectric transition temperature of these compounds is fairly high ( $>900$  K), they have potential use for application, for example, non-volatile ferroelectric memory.<sup>3</sup>

Regarding the magnetism of the Mn moments, they order antiferromagnetically at 70–130 K in the  $120^\circ$  structure,<sup>4–7</sup> which is a typical ordering configuration of triangular antiferromagnets. Since the ferroelectric phase coexists with the antiferromagnetically ordered Mn spins, the coupling between dielectric properties and magnetism is expected in  $RMnO_3$ . In fact, a critical change of dielectric constants at a Néel temperature ( $T_N$ ) is reported in  $RMnO_3$  polycrystals,<sup>8,9</sup> though its mechanism has yet to be understood.

This compound is highly anisotropic both in terms of crystal structure and magnetism, and thus a study of single crystals is indispensable to clarify the detailed physical properties, including the coupling between dielectric properties and the antiferromagnetic ordering. So far, single crystals of these compounds have been made by flux methods,<sup>1</sup> but the size of the crystals, particularly along the  $c$  axis, is not large enough to study the anisotropy of various properties. In this work, we have succeeded in growing single crystals of hex-

agonal  $RMnO_3$  by the floating-zone technique, which are large enough even along the  $c$  axis. This paper reports a comprehensive study of the magnetic, dielectric, structural, and thermal properties of those single crystals.

### II. EXPERIMENT

Polycrystalline rods of  $RMnO_3$  were made by mixing stoichiometric amounts of  $R_2O_3$  ( $R=Y, Yb,$  and  $Lu$ ) and  $MnO_2$  and sintering them at 1200, 1270, and 1350 °C with intermediate grinding. Then, the rod was molten for single-crystal growth with a floating-zone furnace equipped with four halogen lamps. The typical feed speed was 3 mm/h and a typical size of single crystals was 5 mm  $\phi \times 3$  cm. Crystal orientation was determined by back Laue reflection. We also made polycrystalline samples of  $RMnO_3$  including  $R=Sc$  by conventional solid-state-reaction technique. Lattice constants of these samples obtained by x-ray-diffraction measurements are shown in Table I. Magnetic susceptibility was measured by a superconducting quantum interference device magnetometer. Resistivity was measured by conventional four-probe technique, and dielectric constants were measured by a LCR meter. For both measurements, silver paste cured at 800°C was used as electrodes. Specific heat was measured by a relaxation technique. Electron-diffraction measurements were performed using JEM-200CX transmission electron microscope.

### III. TRANSMISSION ELECTRON MICROSCOPY

We first examined the structural features of  $RMnO_3$  at room temperature by transmission electron microscope. Figure 2 shows the electron-diffraction patterns of  $YMnO_3$  at room temperature, with the incident beams parallel to the (a)  $[11\bar{3}]$  and the (b)  $[100]$  direction. It is found that superlattice reflection spots are present at the (110) positions in the reciprocal-lattice space, as shown by arrows in Fig. 2. This indicates that  $YMnO_3$  has a superlattice structure with the  $3a_{330}$  period along the  $[110]$  directions. To elucidate the

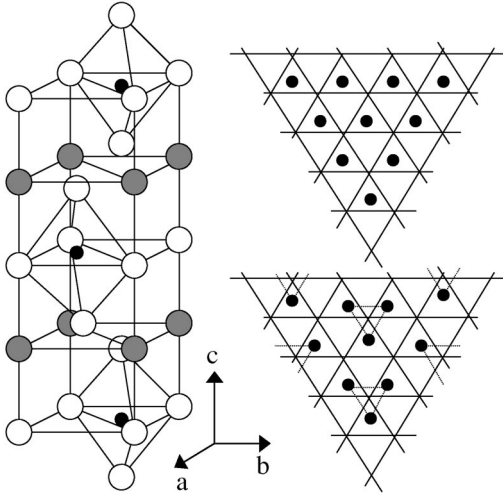


FIG. 1. Left panel: crystal structure of  $\text{LuMnO}_3$ . Black circles correspond to Mn, white circles to O, and gray circles to Lu. Right panel: configuration of the MnO layer. Black circles correspond to Mn, and O is located at the intersection of solid lines. Dotted lines represent the trimers of Mn atoms.

structural feature associated with the superlattice, we took high-resolution (HR) lattice images with the incident beam parallel to the  $[11\bar{3}]$  directions at room temperature, as shown in Fig. 3. Since the  $[11\bar{3}]$  axis is tilted from the  $[001]$  axis only by  $20^\circ$ , the image roughly corresponds to the  $ab$  plane. In the image, bright spots, which form the triangular lattice, and dark spots in between the bright spots, which form the honeycomb lattice, are clearly observed. The bright spots can be assigned to the Mn trimers, as illustrated in the inset of Fig. 3, indicating that the Mn trimer is the main building block of the MnO layers in  $\text{RMnO}_3$ .

Figure 4 shows the dark-field images obtained by the  $(110)$  diffraction spot with different excitations. As can be seen, six kinds of regions with different brightness are observed, which corresponds to six kinds of antiphase domains. Within the triangular-lattice planes with trimerization, three kinds of antiphase domains can be expected. In addition, taking account of two possible ferroelectric polarization vectors ( $z$  and  $-z$ ),  $6 = 3 \times 2$  antiphase domains exist in hexagonal  $\text{RMnO}_3$ , consistent with the experimental result. These results clearly demonstrate the lattice distortion of  $\text{RMnO}_3$  as the combination of the trimerization within the  $ab$  plane and the ferroelectric distortion along the  $c$  axis.

#### IV. MAGNETIC SUSCEPTIBILITY

Figure 5 shows the magnetic susceptibility ( $\chi$ ) of  $\text{RMnO}_3$  single crystals ( $R = \text{Y, Lu}$ ) under the magnetic field (1000

TABLE I. Parameters of structure and magnetism in  $\text{RMnO}_3$ .

$R$	$a$ ( $\text{\AA}$ )	$c$ ( $\text{\AA}$ )	$ \theta $ (K)	$T_N$ (K)	$ \theta /T_N$
Y	6.140(1)	11.393(4)	705	70	10.1
Yb	6.0644(7)	11.380(2)		82	
Lu	6.0480(3)	11.411(1)	887	86	10.3
Sc	5.836(2)	11.170(3)	975	125	7.8

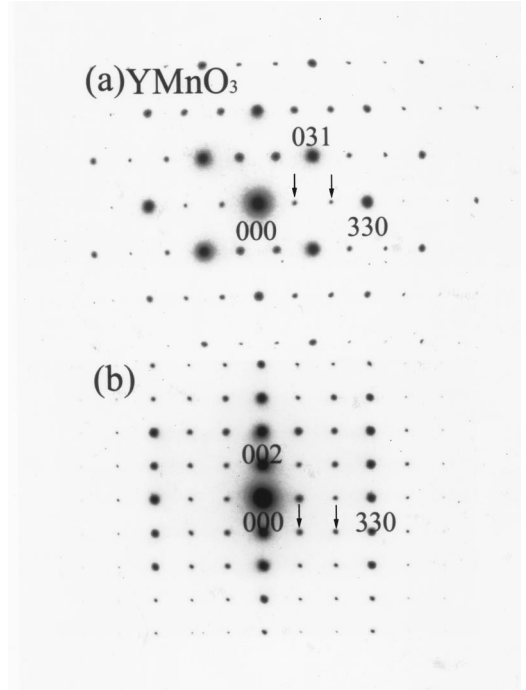


FIG. 2. Electron-diffraction patterns of  $\text{YMnO}_3$  at room temperature. Incident beams are almost parallel to the (a)  $[11\bar{3}]$  and (b)  $[100]$  directions, respectively.

Oe) parallel to the  $ab$  plane ( $\chi_{ab}$ ) and to the  $c$  axis ( $\chi_c$ ), as well as that of polycrystalline  $\text{ScMnO}_3$ . The values of  $\chi_{ab}$  are larger than those of  $\chi_c$  for a whole temperature range, indicating an  $xy$  character of the Mn moment. Previous reports of neutron-scattering measurement<sup>4-7</sup> indicate that the Mn moments lie within the plane in the antiferromagnetic phase, consistent with the present result. At high temperatures (above the cusp shown by arrows),  $\chi(T)$  follows a Curie-Weiss law with a negative Weiss temperature  $\theta$ . We estimated from  $\chi_{ab}$  that  $|\theta|$  is 705, 887, and 975 K for  $R = \text{Y, Lu}$ , and Sc, respectively. These values are discernibly larger than

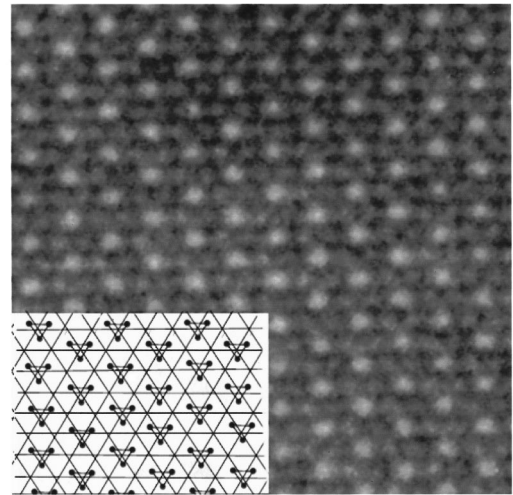


FIG. 3. High-resolution lattice image of  $\text{YMnO}_3$  with the incident beam parallel to the  $[11\bar{3}]$  directions.

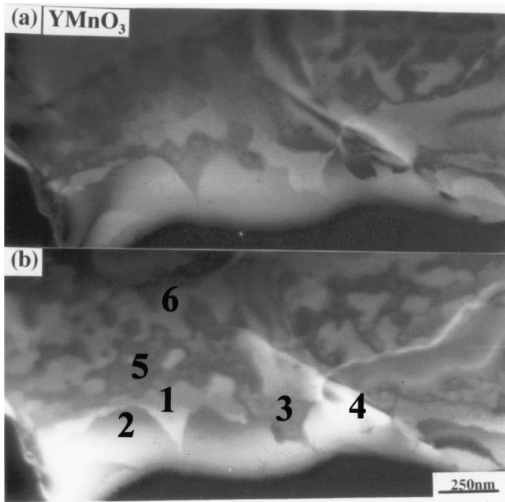


FIG. 4. Dark-field images of  $\text{YMnO}_3$  obtained by the (110) diffraction spot. The upper panel and the lower panel are the images taken with different excitations.

those reported in the previous literature.<sup>7,8</sup> This may be ascribed to the existence of larger number of impurities in the previous polycrystalline samples, which yield an additional Curie term in  $\chi(T)$  and thus causes smaller  $|\theta|$  in the estimation. It should be noted here that the  $|\theta|$  value, which is roughly proportional to the magnitude of the antiferromagnetic interaction between neighboring  $\text{Mn}^{3+}$  ions, increases with decreasing lattice constants, as shown in Table I.

A cusp is clearly observed in  $\chi_c(T)$  of  $\text{YMnO}_3$  (70 K) and  $\text{LuMnO}_3$  (86 K), whereas a sharp increase of  $\chi(T)$  is observed for  $\text{ScMnO}_3$  (125 K), as shown by arrows in Fig. 5, which corresponds to  $T_N$  of each compound. The increase of

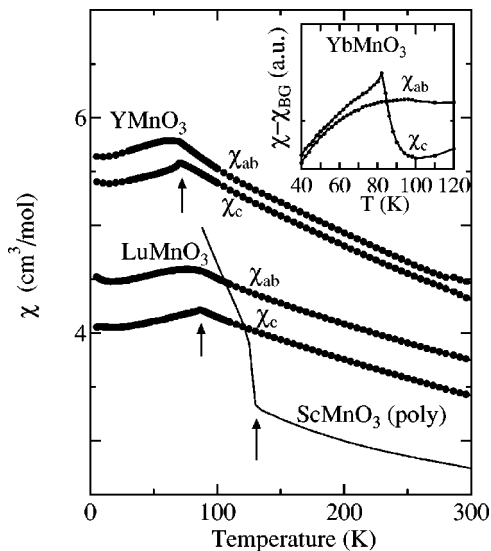


FIG. 5. (a) Magnetic susceptibility ( $\chi$ ) vs temperature for single crystals ( $R = \text{Y}$  and  $\text{Lu}$ ) and a polycrystal ( $R = \text{Sc}$ ) of  $\text{RMnO}_3$ .  $\chi_{ab}$  and  $\chi_c$  represent the data with magnetic field parallel to the  $ab$  plane and the  $c$  axis, respectively. Arrows show Néel temperatures. The inset shows the data of  $\text{YbMnO}_3$ , where the contribution from the Yb moment has been subtracted.

$\chi(T)$  in  $\text{ScMnO}_3$  below  $T_N$  is caused by weak ferromagnetism, which is likely to be dominated by Dzialonshinskii-Moriya interaction.<sup>7</sup> It should be stressed here that  $T_N$  is much smaller than  $|\theta|$  in these compounds. As discussed in Sec. I, these compounds have the Mn triangular-lattice layers, and thus strong geometrical frustration of antiferromagnetically coupled Mn spins is expected. It is known that the ratio of  $T_N$  to  $|\theta|$  is a good measure of the spin frustration, and if  $|\theta|/T_N$  is larger than 10, the spin system should be classified as the one with strong geometrical frustration, since the value cannot be explained by a simple mean-field theory.<sup>10</sup> On the basis of the values of  $|\theta|$  and  $T_N$  estimated in the present study, the ratio of  $T_N$  to  $|\theta|$  is  $\sim 10$ , as summarized in Table I. Therefore it is proposed here that hexagonal  $\text{RMnO}_3$  is a spin system with strong geometrical frustration, similarly with  $\text{SrCr}_9\text{Ga}_{12-9p}\text{O}_{19}$ ,<sup>11</sup>  $\text{ZnCr}_2\text{O}_4$ ,<sup>12</sup> and  $\text{ZnV}_2\text{O}_4$ .<sup>13</sup>

For  $\text{YMnO}_3$  and  $\text{LuMnO}_3$ , one notices that a definite cusp at  $T_N$  is observed only in  $\chi_c(T)$ , whereas a least anomaly at  $T_N$  followed by a broad peak at  $T < T_N$  is observed in  $\chi_{ab}(T)$ . Such anisotropy around  $T_N$  is more pronounced for  $\text{YbMnO}_3$ , where  $\chi_c(T)$  shows a sharp peak but  $\chi_{ab}(T)$  has no anomaly at  $T_N$ , as shown in the inset of Fig. 5. Since the easy axis of the Mn moment is along the  $ab$  plane, the difference between  $\chi_{ab}(T)$  and  $\chi_c(T)$  cannot be explained only by single-ion anisotropy. It is known that  $\text{VBr}_2$  with a similar triangular-lattice structure shows also a broad peak around  $T_N$  for both  $\chi_{ab}(T)$  and  $\chi_c(T)$ .<sup>14</sup> Thus it is likely that the broad peak of  $\chi_{ab}(T)$  in  $\text{RMnO}_3$  is the intrinsic behavior of the triangular-lattice layers, but the cusp of  $\chi_c(T)$  is caused by another origin. Taking account of the experimental result that the anomaly of  $\chi_c(T)$  is more pronounced in  $\text{YbMnO}_3$  containing additional  $\text{Yb}^{3+}$  moments between Mn triangular-lattice layers, an interlayer coupling between two adjacent Mn layers can be a possible origin for the  $\chi_c(T)$  anomaly.

## V. RESISTIVITY AND DIELECTRIC CONSTANT

Temperature dependence of the resistivity of  $\text{RMnO}_3$  single crystals for  $R = \text{Y}$ ,  $\text{Yb}$ , and  $\text{Lu}$  is shown in Fig. 6. As can be seen, resistivity increases with decreasing temperature for all compounds, and the anisotropy between in-plane and out-of-plane resistivity is  $10^1 - 10^2$ , indicating a modest two-dimensional character of their electronic structures. The size of the resistivity anisotropy is smaller than that of  $\text{La}_{1-x}\text{Sr}_{1+x}\text{MnO}_4$  with  $\text{K}_2\text{NiF}_4$  structure ( $\sim 10^3$ ),<sup>15</sup> probably because the distance between the neighboring Mn layers along the  $c$  axis of  $\text{RMnO}_3$  ( $\sim 5.7 \text{ \AA}$ ) is smaller than that of  $\text{La}_{1-x}\text{Sr}_{1+x}\text{MnO}_4$  ( $\sim 6.2 \text{ \AA}$ ). At the ferroelectric transition temperature (for example, 910 K for  $\text{YMnO}_3$ ), one can barely see the anomaly of resistivity, which is in contrast to a drastic change of resistivity in perovskite  $\text{LaMnO}_3$  associated with the structural phase transition at 750 K.<sup>16</sup> There is no systematic rare-earth dependence of resistivity, but fairly large sample dependence among the same composition exists, as demonstrated for two samples of  $\text{YbMnO}_3$  from different batches. We speculate that such strong sample dependence of resistivity values is due to oxygen offstoichiometry.

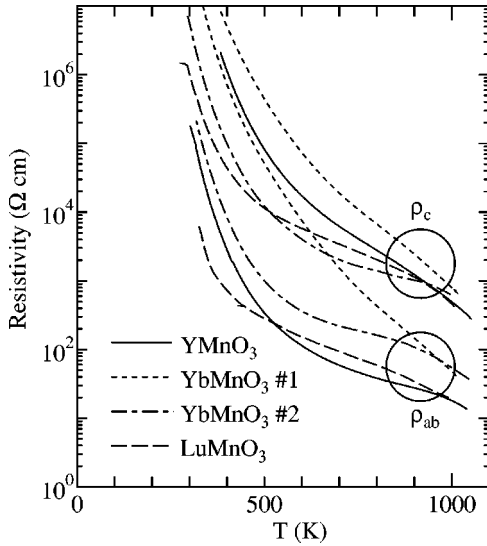


FIG. 6. Temperature dependence of resistivity for  $\text{YMnO}_3$ ,  $\text{YbMnO}_3$ , and  $\text{LuMnO}_3$ . Two samples of  $\text{YbMnO}_3$  are from different batches.

Figure 7 shows the low-temperature dielectric constant [ $\epsilon(T)$ ] of  $\text{RMnO}_3$  single crystals for  $R=\text{Y}$  and  $\text{Lu}$  at 100 kHz. The dielectric loss is zero within the experimental error in this temperature range ( $<150$  K). A critical decrease of the dielectric constant with the electric field along the  $ab$  plane ( $\epsilon_{ab}$ ) can be seen at  $T_N$  for both  $\text{YMnO}_3$  and  $\text{LuMnO}_3$ . An additional peak of  $\epsilon(T)$  at  $T < T_N$  was reported in early literature,<sup>8,9</sup> which is also observed in some of our polycrystalline samples (shown by a closed triangle in Fig. 7). However, the peak is absent in all single crystals, suggesting that the peak at  $T < T_N$  is caused by the grain-boundary effect.

It can also be seen that the anomaly at  $T_N$  is absent when the electric field is along the  $c$  axis ( $\epsilon_c$ ). Such anisotropy of the dielectric constant [an anomaly in  $\epsilon_{ab}(T)$  but no anomaly in  $\epsilon_c(T)$ ] is in clear contrast to that of the magnetic susceptibility [a cusp in  $\chi_c(T)$  but no anomaly in  $\chi_{ab}(T)$ ], implying

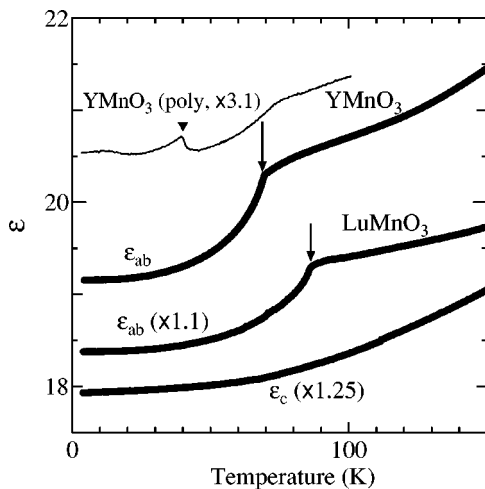


FIG. 7. Dielectric constants of  $\text{YMnO}_3$  and  $\text{LuMnO}_3$ . Arrows show Néel temperatures. Data are multiplied by constants for clarity.

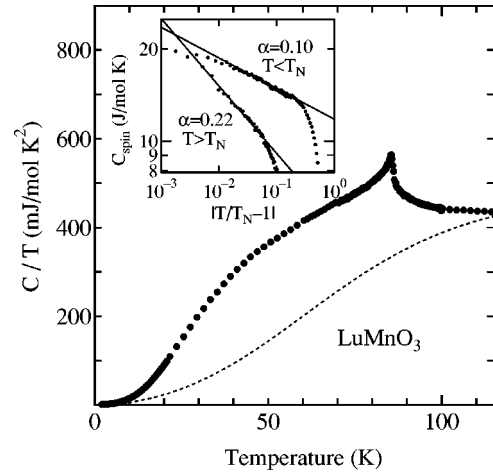


FIG. 8. Specific heat divided by temperature for  $\text{LuMnO}_3$ . The dashed line is the acoustic-phonon contribution (see text). The inset shows the  $C_{\text{spin}}$  vs  $|T/T_N - 1|$  in a log-log plot to estimate a critical exponent  $\alpha$ .

a unique correlation between the dielectric and magnetic properties in these compounds. An anomaly of  $\epsilon_{ab}(T)$  at  $T_N$  and its absence in  $\epsilon_c(T)$  suggest that it is dominated by some interaction within the  $ab$  plane. This issue will be discussed in a later section.

## VI. SPECIFIC HEAT

The specific heat of  $\text{LuMnO}_3$  divided by temperature is shown in Fig. 8, where a  $\lambda$ -type anomaly is observed at  $T_N$ . According to the scaling theory,  $C_{\text{spin}}$  in the vicinity of  $T_N$  behaves like  $C_{\text{spin}} = A|t|^{-\alpha}$  with  $t = T/T_N - 1$ . To experimentally obtain the critical exponent  $\alpha$ , phonon contribution has to be estimated and subtracted from the total specific heat. As an estimation of phonon contribution, we use a Debye formula,

$$C_{\text{lattice}} = 3RN \cdot 3 \left( \frac{T}{\theta_D} \right)^3 \int_0^{\theta_D/T} \frac{\zeta^4 e^{\zeta} d\zeta}{(e^{\zeta} - 1)^2}, \quad (1)$$

where  $R$  is the gas constant,  $N$  the number of atoms per unit cell ( $=5$ ), and  $\theta_D$  is a Debye temperature. We chose  $\theta_D = 550$  K so that the experimental value of  $C$  at 120 K (the upper limit of our experiment) coincides with  $C_{\text{lattice}}$ , as shown by a dashed line in Fig. 8. Spin specific heat  $C_{\text{spin}}$  was obtained by subtracting this lattice contribution from the measured specific heat. The critical exponent  $\alpha$  was estimated from the log-log plot of  $C_{\text{spin}}$  vs  $|T/T_N - 1|$ , as shown in the inset of Fig. 8. The experimentally obtained  $\alpha$  is  $\sim 0.22$  for  $T > T_N$  and 0.10 for  $T < T_N$ . Such discrepancy of  $\alpha$  above and below  $T_N$  is not consistent with the scaling theory, but is often observed experimentally.<sup>17</sup> We speculate that the randomness existing in the real compounds modifies the critical behavior from its ideal one. Note that the peak of  $C(T)$  at  $T_N$  for the polycrystalline samples of  $\text{RMnO}_3$  (Ref. 7) is more rounded than the present result for a single crystal, probably because polycrystalline samples have more randomness than single crystals.

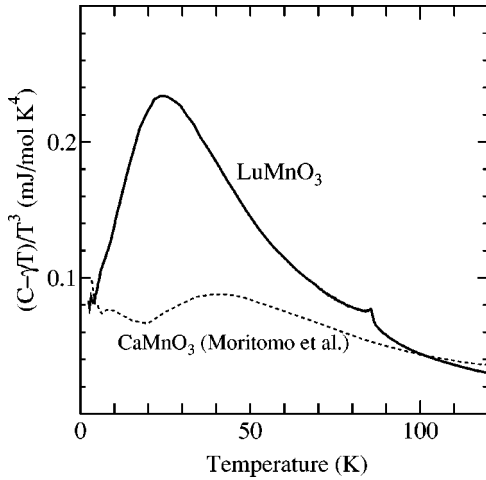


FIG. 9.  $(C - \gamma T)/T^3$  vs temperature for  $\text{LuMnO}_3$  (the solid line) and  $\text{CaMnO}_3$  (the dotted line).  $\gamma$  is 1.0 mJ/mol  $\text{K}^2$ , and 2.3 mJ/mol  $\text{K}^2$  for  $\text{LuMnO}_3$  and  $\text{CaMnO}_3$ , respectively.

One may notice that the spin entropy of  $\text{LuMnO}_3$  given by the subtraction of the phonon contribution (a dashed line) from the total entropy (closed circles) has large residual weight at low temperatures. This can be more clearly seen with less ambiguity in Fig. 9, where  $[C(T) - \gamma T]/T^3$  ( $\gamma$  is a  $T$ -linear coefficient of specific heat) is plotted. As discussed above, the contribution of acoustic phonon can be given by the Debye formula, which gives a  $T^3$  term at low temperatures and then saturated near the Debye temperature  $\theta_D$ . A similar behavior is expected for antiferromagnetic magnon, which also produces the same contribution to specific heat as acoustic phonon. Therefore, if  $[C(T) - \gamma T]/T^3$  is plotted for conventional antiferromagnets, it is constant up to a certain temperature and then decreases with further increasing temperature. This is experimentally the case for a conventional antiferromagnet  $\text{CaMnO}_3$  with  $S = 3/2$  on the cubic lattice,<sup>18</sup> as shown by the dashed line in Fig. 9. However,  $[C(T) - \gamma T]/T^3$  has a clear peak around 25 K for  $\text{LuMnO}_3$  as seen in the same figure. This means that low-temperature specific heat has a strong deviation from the  $T^3$  rule. It is likely that this peak comes from the geometrical frustration existing in the triangular lattice. In conventional antiferromagnets, most of the spin entropy disappears around  $T_N$  and only magnon contribution survives at low temperatures, whereas a part of the spin moment seems to be fluctuating down to low temperatures in hexagonal  $\text{RMnO}_3$ . According to a neutron-scattering measurement, the antiferromagnetic moment of  $\text{RMnO}_3$  [ $2.9\mu_B$  for  $\text{YMnO}_3$  (Ref. 7)] is discernibly smaller than the expected value for  $\text{Mn}^{3+}$ ,  $4\mu_B$ . One possible interpretation is that the missing moment is fluctuating down to low temperatures owing to the geometrical frustration, and is responsible for the peak around 25 K in  $[C(T) - \gamma T]/T^3$ .

## VII. DISCUSSION

First of all, we discuss the mechanism of the change of dielectric constants at  $T_N$ . Since the anomaly is observed only in  $\epsilon_{ab}(T)$ , it is unlikely to be dominated by the change of the ferroelectric polarization or relating optical phonons

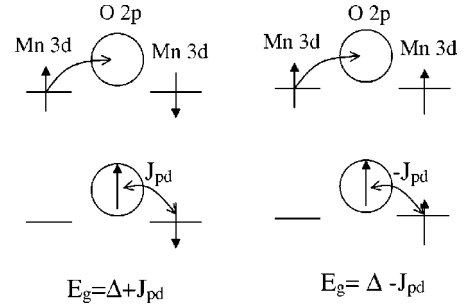


FIG. 10. Illustration of the process of in-plane charge-transfer excitation with  $p$ - $d$  exchange interaction ( $J_{pd}$ ) for antiferromagnetic (left) and ferromagnetic (right) ordering of the Mn moments.

moving along the  $c$  axis, but likely to be dominated by in-plane magnetic interaction. The dc dielectric constant is dominated both by electronic excitations and phononic excitations, but here, we only take account of electronic excitations for dielectric constants. In the analogy with perovskite manganites, the lowest in-plane charge excitation is the charge-transfer excitation between the Mn  $3d$  state and the in-plane oxygen  $2p$  state.<sup>19</sup> Since the relation between a dc dielectric constant ( $\epsilon$ ) and a charge excitation gap ( $E_g$ ) is roughly given by  $\epsilon = 1/E_g^2$ , the decrease of dielectric constants with antiferromagnetic ordering means the increase of the excitation gap. A change of an excitation gap with magnetic ordering is observed in Eu chalcogenides,<sup>20</sup> and in its analogy, we can explain the change of the dielectric constant of  $\text{RMnO}_3$  with magnetic ordering as follows: the Mn  $3d$  state and the oxygen  $2p$  state, and the exchange spin interaction between these two states ( $J_{pd}$ ) are assumed. It is expected that  $J_{pd}$  is ferromagnetic, judging from the experimental results that doped holes in perovskite manganites favor ferromagnetic alignment. As discussed above, the lowest excitation in  $\text{RMnO}_3$  is the one to move a hole from the Mn site to the in-plane oxygen site. If the energy difference between these two states (Mn  $3d$  and oxygen  $2p$ ) is  $\Delta$ , the final-state energy is  $\Delta - J_{pd}$  when the Mn moments are ferromagnetically aligned, and  $\Delta + J_{pd}$  when antiferromagnetically aligned, as illustrated in Fig. 10. In such a situation, the energy gap increases and thus the dielectric constant decreases with the transition from a paramagnetic phase (with randomly oriented spins) to an antiferromagnetic phase. From the magnitude of the change of the dielectric constant, it can be estimated that  $J_{pd}$  of  $\text{RMnO}_3$  is several % of the charge gap ( $\sim$  eV), i.e., several tens meV, in spite of low  $T_N$  ( $k_B T_N = 6$  meV for  $\text{YMnO}_3$ ). It should be pointed out that if  $T_N$  were so high so that the effect of thermally excited carriers cannot be ignored, such a sharp decrease of the dielectric constant would not be observed. Therefore a large and sharp decrease of the dielectric constant at  $T_N$  in  $\text{RMnO}_3$  is partly due to geometrical frustration, i.e., much lower  $T_N$  compared with typical energy scale of magnetic interaction. It should be pointed out that magnetic ordering does not affect the charge-transfer excitation between the Mn state and the apical oxygen state based on the present model, resulting in the absence of the anomaly in  $\epsilon_c(T)$  at  $T_N$ , consistent with the experiment.

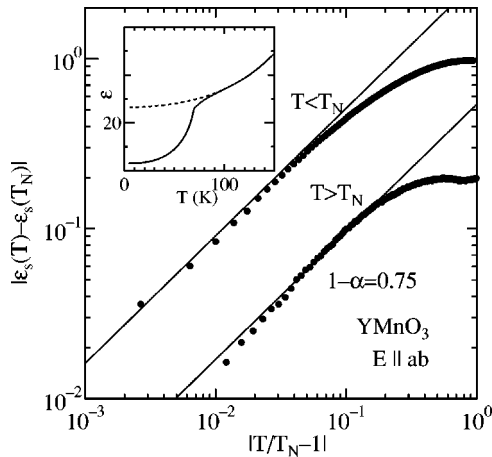


FIG. 11.  $|\epsilon_s(T) - \epsilon_s(T_N)|$  vs  $|T/T_N - 1|$  for the estimation of a critical exponent  $\alpha$  of  $\text{YMnO}_3$ . Solid lines correspond to the fitting to  $\alpha = 0.25$ . The dotted line in the inset shows the estimated lattice contribution.

The argument above implies that the dominant factor for the change of  $\epsilon(T)$  is  $\langle S_i \cdot S_j \rangle$ , where  $i$  and  $j$  denote the neighboring Mn sites. Thus  $\epsilon_s(T)$ , which is the dielectric constant subtracted by the temperature-dependent lattice contribution, should behave like  $|\epsilon_s(T) - \epsilon_s(T_N)| = A|t|^{1-\alpha}$ , where  $t = T/T_N - 1$  and  $\alpha$  is the same as that of specific heat, in the vicinity of  $T_N$ .<sup>21</sup> We estimated the critical exponent  $\alpha$  by fitting  $\epsilon_{ab}(T)$  of  $\text{YMnO}_3$  as shown in Fig. 11, and found  $\alpha \sim 0.25$  for both above and below  $T_N$ . This value is almost consistent with that estimated from specific heat for  $T > T_N$ . A Monte Carlo simulation estimates that a critical exponent  $\alpha$  of  $xy$  antiferromagnet on the triangular lattice is  $0.40 \pm 0.10$ ,<sup>22</sup> and our result is evidently out of the error bar. A possible reason for the discrepancy is the randomness effect as discussed in Sec. VI. Another one is the trimerization of the Mn ions, which breaks the symmetry of the triangular

lattice and thus stabilizes a  $120^\circ$  structure with specific chirality.<sup>22</sup>

## VIII. SUMMARY

Magnetic, dielectric, structural, and thermal properties were investigated for single crystals of hexagonal  $\text{RMnO}_3$  ( $R = \text{Y, Yb, and Lu}$ ), which contains triangular-lattice layers of Mn ions. We have observed the formation of Mn trimers in a high-resolution real space image of transmission electron microscope. Regarding the magnetism of these compounds, the ratio of a Weiss temperature to  $T_N$  is  $\sim 10$ , indicating strong geometrical frustration of these compounds. Specific heat shows a  $\lambda$ -type anomaly at  $T_N$  as well as a clear deviation from a  $T^3$  rule at low temperatures, indicating that spin fluctuation survives far below  $T_N$  because of geometrical frustration of the Mn triangular lattice. It is also found that a cusp of magnetic susceptibility at  $T_N$  appears only for  $\chi_c(T)$  but not for  $\chi_{ab}(T)$ . On the other hand, a critical decrease of dielectric constants ( $\epsilon$ ) at  $T_N$  occurs only for  $\epsilon_{ab}(T)$  but not for  $\epsilon_c(T)$ , in clear contrast to the behavior of magnetic susceptibility. The decrease of  $\epsilon_{ab}(T)$  at  $T_N$  can be explained by a spin-dependent charge-transfer gap between Mn  $3d$  and in-plane oxygen  $2p$  states with strong  $p$ - $d$  exchange interaction. Attempts to estimate a critical exponent  $\alpha$  were made on the data of specific heat and dielectric constants, which gave values not fully consistent with theories, probably because of the existence of randomness in the samples. This system can be regarded as a ferroelectric/frustrated-spin hybrid, which gives us a unique opportunity to study the coupling between dielectric properties and spins with geometrical frustration.

## ACKNOWLEDGMENT

The present work was partly supported by a Grant-In-Aid for Scientific Research from the Ministry of Education, Science, and Culture, Japan.

- <sup>1</sup>H. L. Yakel and W. C. Koehler, *Acta Crystallogr.* **16**, 957 (1963).
- <sup>2</sup>I. G. Ismailzade and S. A. Kizhaev, *Fiz. Tverd. Tela* **7**, 298 (1965) [*Sov. Phys. Solid State* **7**, 236 (1965)].
- <sup>3</sup>H. Kitahata, K. Tadanaga, T. Minami, N. Fujimura, and T. Ito, *Appl. Phys. Lett.* **75**, 719 (1999), and references therein.
- <sup>4</sup>E. F. Bertaut and M. Mercier, *Phys. Lett.* **5**, 27 (1963).
- <sup>5</sup>W. C. Koehler, H. L. Yakel, E. O. Wollan, and J. W. Cable, *Phys. Lett.* **9**, 93 (1964).
- <sup>6</sup>M. Bieringer and J. E. Greedan, *J. Solid State Chem.* **143**, 132 (1999).
- <sup>7</sup>A. Muñoz, J. A. Alonso, M. J. Martínez-Lope, M. T. Casáis, J. L. Martínez, and M. T. Fernández-Díaz, *Phys. Rev. B* **62**, 9498 (2000).
- <sup>8</sup>Z. J. Huang, Y. Cao, Y. Y. Sun, Y. Y. Xue, and C. W. Chu, *Phys. Rev. B* **56**, 2623 (1997).
- <sup>9</sup>N. Iwata and K. Kohn, *J. Phys. Soc. Jpn.* **67**, 3318 (1998).
- <sup>10</sup>P. Schiffer and A. P. Ramirez, *Comments Condens. Matter Phys.* **18**, 21 (1996).
- <sup>11</sup>A. P. Ramirez, B. Hessen, and M. Winklemann, *Phys. Rev. Lett.* **84**, 2957 (2000).
- <sup>12</sup>S.-H. Lee, C. Broholm, T. H. Kim, W. Ratcliff, II, and S.-W.

- Cheong, *Phys. Rev. Lett.* **84**, 3718 (2000).
- <sup>13</sup>S. Kondo, C. Urano, Y. Kurihara, M. Nohara, and H. Takagi, *J. Phys. Soc. Jpn.* **69**, Suppl. B 139 (2000).
- <sup>14</sup>K. Hirakawa, H. Ikeda, H. Kadowaki, and K. Ubukoshi, *J. Phys. Soc. Jpn.* **52**, 2882 (1983).
- <sup>15</sup>Y. Moritomo, Y. Tomioka, A. Asamitsu, Y. Tokura, and Y. Matsui, *Phys. Rev. B* **51**, 3297 (1995).
- <sup>16</sup>J.-S. Zhou and J. B. Goodenough, *Phys. Rev. B* **60**, R15 002 (1999).
- <sup>17</sup>K. Takeda, N. Uryû, K. Ubukoshi, and K. Hirakawa, *J. Phys. Soc. Jpn.* **55**, 727 (1986).
- <sup>18</sup>Y. Moritomo, A. Machida, E. Nishibori, M. Takata, and M. Sakata (unpublished).
- <sup>19</sup>Y. Okimoto, T. Katsufuji, T. Ishikawa, T. Arima, and Y. Tokura, *Phys. Rev. B* **55**, 4206 (1997).
- <sup>20</sup>A. Mauger and C. Godart, *Phys. Rep.* **141**, 51 (1986).
- <sup>21</sup>A similar estimation of a critical exponent  $\alpha$  was carried out by fitting the spin-dependent birefringence of  $\text{RbMnBr}_3$  [T. Kato, K. Iio, T. Hoshino, T. Mitsui, and H. Tanaka, *J. Phys. Soc. Jpn.* **61**, 275 (1992)].
- <sup>22</sup>H. Kawamura, *J. Phys. Soc. Jpn.* **58**, 584 (1989).